Quadrupole moment of the yrast superdeformed band in ^{192}Pb

A.N. Wilson [a,b,*], G.D. Dracoulis [a], P.M. Davidson [a], A.P. Byrne [a,b],
R.M. Clark [c], P. Fallon [c], A. Görgen [c,1], G.J. Lane [a],
A.O. Macchiavelli [c], D. Ward [c]

[a] *Department of Nuclear Physics, Research School of Physical Sciences and Engineering,
Australian National University, Canberra ACT 0200, Australia*
[b] *Department of Physics, Faculty of Science, Australian National University, Canberra ACT 0200, Australia*
[c] *Nuclear Science Division, Lawrence Berkeley National Laboratory, Berkeley, CA, USA*

Abstract

The lifetimes of states with spins $26\hbar \geqslant I \geqslant 18\hbar$ in the yrast superdeformed band of ^{192}Pb have been measured using the Doppler shift attenuation method. The results are consistent with a constant quadrupole moment $\langle Q_0 \rangle = 19.6^{+0.5}_{-0.4}(\text{stat}) \pm 2.0(\text{sys})$ eb. This result is comparable with the values obtained for SD bands in Pb isotopes with $N \geqslant 112$, but could also be consistent with the smaller quadrupole moment measured in ^{193}Pb. Reasons for the apparently lower deformation of SD ^{193}Pb (compared to its heavier neighbours) are considered in the light of total Routhian surface calculations, and the question of whether a similarly reduced deformation should be expected in ^{192}Pb is addressed.

---

* Corresponding author.
  E-mail address: anna.wilson@anu.edu.au (A.N. Wilson).
[1] Present address: CEA Saclay, DAPNIA/SPhN, Bat. 703, l'Orme des Merisiers, F-91191 Gif-sur-Yvette, France.

1. Introduction

1.1. Motivation for lifetime measurements in superdeformed nuclei

The first evidence for an island of superdeformation around mass number $A \approx 190$ came with the observation of a superdeformed band in ^{191}Hg by Moore et al. [1] in 1989. Since then, 83 superdeformed rotational bands have been observed in this mass region in 25 isotopes of Au, Hg, Tl, Pb, Bi and Po [2]. It is well established that the superdeformed minimum in this region is associated with the presence of $N = 6$ ($i_{13/2}$) proton and $N = 7$ ($j_{15/2}$) neutron intruder orbitals, which are close to the Fermi surface at large deformations. However, the precise order of the orbitals close to the Fermi surface, and whether or not the number of *occupied* intruder orbitals polarizes the nuclear shape, is not known.

Unfortunately, the experimental evidence needed to determine the microscopic structure of SD bands has been very limited, mainly because of the difficulty of connecting the SD bands into the normal level scheme. Direct linking transitions between SD and ND states, which allow absolute excitation energies, spins and parities to be established, have been observed in only a handful of cases [3–7] in this mass region. With the exception of an excited band in ^{194}Hg [4], all of the SD bands for which excitation energies have been measured are the yrast bands in even–even nuclei, and are therefore associated with the superdeformed "vacuum" state. The superdeformed states in nuclei with $A \approx 190$ occur at sufficiently low spins that the SD nuclei are strongly affected by pairing correlations, and so the SD vacuum is not simply described in a single-particle picture. Thus even where this detailed information is available, little light has been shed on the underlying nuclear structure.

Uniquely in this mass region, it has been possible to obtain strong evidence for a particular configuration assignment in those cases where g-factors can be extracted for signature partner bands [8–11]. However, such information is limited to those cases where both in- and inter-band transitions are observed: that is, to odd-A nuclei where the valence nucleon occupies a relatively high-K orbital.

One other way in which information has been gleaned about the underlying single-particle configurations is through the measurement of the lifetimes of the in-band superdeformed transitions. With the construction of the high-efficiency γ-ray detector arrays Gammasphere and Euroball, it has been possible to perform comparative measurements, in which several SD bands are populated via reactions on a single target, and their lifetimes measured using the Doppler shift attenuation method (DSAM). Such experiments allow the lifetimes of states with comparable properties to be measured with good relative precision, despite the large uncertainty (of the order of 10% [12]) in the stopping powers. As the intruder orbitals are primarily responsible for the formation of the superdeformed minimum, it might be expected that the higher the number of intruder orbitals occupied in a particular SD band, the larger the nuclear deformation. It was hoped that measurements of the quadrupole moments of SD bands across an isotopic chain, or of different SD bands

within the same nucleus, would be sensitive to the polarizing effects of the active neutron and proton single-particle orbitals and would thus provide insight into the configurations supporting different SD bands.

1.2. Comparative lifetime measurements in the $A \approx 190$ region

Comparative measurements of the lifetimes of SD bands have been carried out in several nuclei in the $A \approx 190$ region of superdeformation. Moore et al. used this method to measure the lifetimes of yrast and excited SD bands in ^{192}Hg and ^{194}Hg [13]; Busse et al. measured the lifetimes of yrast and excited SD bands in ^{192}Hg and ^{193}Hg [14]; van Severen et al. measured the lifetimes of the yrast SD bands in each of the Pb isotopes with neutron number $111 \leqslant N \leqslant 114$ [15]; and recently, Rossbach et al. made a simultaneous measurement of the lifetimes of yrast and excited SD bands in ^{196}Pb [16].

The excited SD bands ^{192}Hg, ^{194}Hg and ^{196}Pb are based on octupole vibrational states [17] and thus the difference in the quadrupole deformation of the zero and one-phonon states should be minimal. The experimental measurements are consistent with the vibrational interpretation and thus do not provide information on the shape-polarizing effects of specific orbitals.

The comparative studies of bands in ^{192}Hg and ^{193}Hg and of yrast SD bands in the Pb isotope chain, on the other hand, might be expected to reveal shape-polarizing effects if they are present. The Hg study suggested that the active single-particle orbitals (primarily $N = 5$ and $N = 7$ neutron orbitals) have only a small influence on the degree of deformation. In contrast, the results of the Pb study suggested that the number of occupied $N = 7$ intruder orbitals has a marked effect on the SD deformation. The question of the degree to which the SD shape is governed by the occupation of particular single-particle orbitals is thus one which deserves further attention.

1.3. DSAM measurement of SD ^{192}Pb

This paper reports on a DSAM measurement of the lifetimes of states in the yrast band in ^{192}Pb. The results of this measurement are used to infer an average quadrupole moment of $19.6^{+0.5}_{-0.4} \pm 2.0$ eb, where the first error reflects the statistical uncertainty in the measurement and the second the uncertainty due to the stopping powers. This result is comparable with the measured quadrupole moments of the yrast SD bands in Pb isotopes with $N \geqslant 112$; however, different experimental and analysis conditions between the current measurement and the previous study of Pb isotopes [15] mean that there is the possibility of some systematic difference, and when the uncertainties in the stopping powers are taken into account, the result is also consistent with the measurement of ^{193}Pb. The reasons for the reduced quadrupole moment in ^{193}Pb, and whether or not a reduced quadrupole moment should also be expected in ^{192}Pb, are considered.

2. Experimental details

High-spin states in ^{192}Pb were populated in the ^{29}Si(^{168}Er, 5n) reaction at a beam energy of 154 MeV. The beam was provided by the 88" Cyclotron at the Lawrence Berkeley

National Laboratory. Two targets were used: (i) a 1 mg/cm^2 layer of ^{168}Er on a 5 mg/cm^2 backing layer of Pb and (ii) a self-supporting foil of ^{168}Er of thickness 1 mg/cm^2. The targets were placed at the focal point of the Gammasphere multi-detector array [18], which was used to measure γ-ray coincidences. For this experiment, the array consisted of 101 large-volume escape-suppressed Ge detectors situated at the following angles relative to the beam direction: 17.3°, 31.7°, 37.4°, 50.1°, 58.3°, 69.8°, 79.2°, 80.7°, 90.0°, 99.3°, 100.8°, 110.2°, 121.7°, 129.9°, 142.6°, 148.3° and 162.7°. When target (i) was in place, the Pb evaporation residues were slowed and stopped in the Pb backing; when target (ii) was in place, they recoiled into vacuum. An event was written to tape when at least three signals were obtained from the Ge detectors after escape suppression. Detector identification, incident energy and time (relative to the RF signal of the Cyclotron) were written to tape. In a measuring time of approximately 3.5 days, a total of 6.3×10^8 three- and higher-fold events were collected with target (i) and 2.4×10^8 three- and higher-fold events with target (ii).

3. Initial analysis

In the offline analysis of the data taken with target (i) (the backed target), triple-gated SD spectra were obtained for each of the rings of detectors in the array by requiring that at least three SD transitions were detected in any other detector. Care was taken to ensure that each gate encompassed the full line shape of the γ-ray transition. The gating transitions used in the analysis were the 215, 262, 304, 345, 385, 424, 462 and 499 keV SD transitions. Although the last two of these gates overlap with intensely populated transitions of energies 463, 502 and 504 keV in the lower-spin part of the normal level scheme, it was found that very few contaminant peaks were introduced in the triple-gated spectrum and, as the band is in coincidence with these lower-lying transitions, they were retained as gates. Double-gated spectra were also created following the same procedure: these spectra were used to allow a background-subtraction to be carried out. The background-subtracted, triple-gated spectra obtained in this manner for the two rings of detectors at $\theta = 37°$ and $\theta = 142°$ are shown in Fig. 1, along with the SD level scheme. The stopped peaks from the low-lying part of the level scheme fed by the decay of the SD band are visible in these spectra at 502, 504, 565 and 854 keV.

In order to carry out a DSAM analysis, it is necessary to know what fraction of the population of each level is due to side-feeding. Because of the large width of the higher-energy peaks in the backed-target data and the resulting overlap with transitions in other parts of the level schemes, the intensity profile of the band (and thus the intensity of side-feeding at each level) was obtained from the data obtained with target (ii) (the self-supporting target). Measurement of the intensity profile of the band in these data proved more straightforward, since the SD transitions were better separated from contaminants and the results of multiple-peak fits were more reliable. In addition, the better separation of the peaks made it possible to use double-gated spectra, and the associated higher statistics allowed the measurement of a more accurate intensity profile. A spectrum obtained by doubling gating on the SD band in these data is shown in Fig. 2.
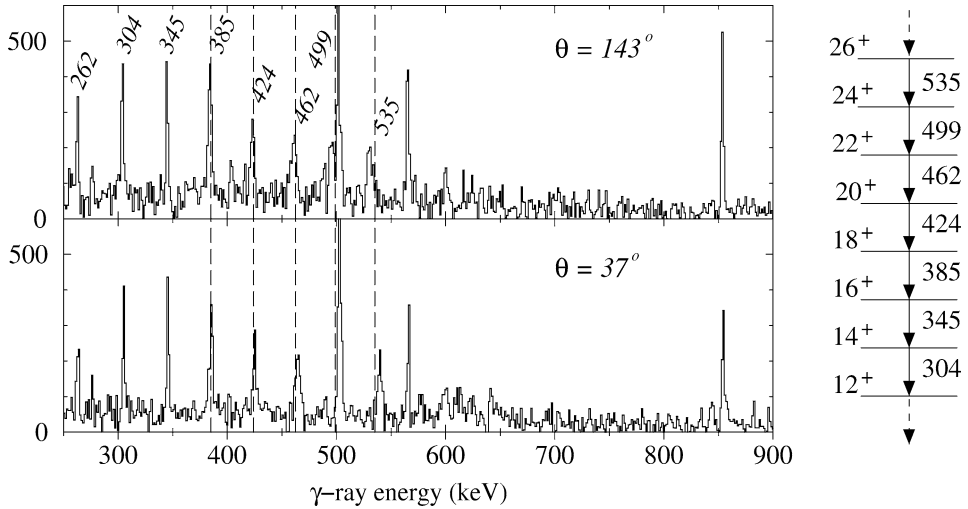
Fig. 1. Background-subtracted triple-SD-gated spectra detected at angles of $\theta = 142°$ (upper panel) and $\theta = 37°$ (lower panel) with respect to the beam direction. Peaks belonging to the SD band are marked with their unshifted energies. The vertical dashed lines indicate the positions of these energies. The level scheme of the SD band is shown on the right-hand side, indicating the spins of the levels connected by each γ ray.
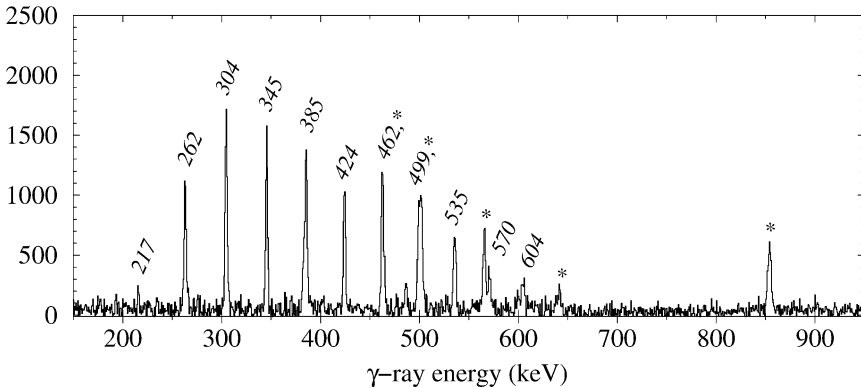

Fig. 2. Double-gated spectrum obtained from the thin-target data. Gates have been set on all double combinations of the 262, 304, 345 and 385 keV SD transitions. In-band SD transitions are marked with their energies. Transitions marked with stars are from low-lying levels in ^{192}Pb which are fed by the decay of the SD band.

4. Lifetimes analysis

In previous DSAM measurements in this mass region, two methods have been used to extract the lifetimes of states within the SD bands. At high spins, where the SD band is directly populated and the transition energies are relatively high, the levels decay extremely rapidly and the corresponding peaks contain only a fully-shifted component. In these circumstances, a centroid-shift approach is appropriate: such measurements have been carried out for the yrast bands in the heavier Pb isotopes with $N = 111$–114 [15,

16]. At lower spins, where the transition energies are lower and thus the lifetimes longer, a lineshape analysis is required. In this region, the peaks contain contributions from fully-shifted, partially-shifted and, towards the bottom of the band, fully-stopped components. Because of the greater fissility of this neutron-deficient nucleus, the band was only weakly-populated at high spins, and thus all observed transitions were in this latter region. It was thus not possible to perform a centroid-shift analysis in the present work. A lineshape analysis was employed to measure the lifetimes of the states in the yrast SD band with spins $26\hbar \geqslant I \geqslant 18\hbar$ (at lower spins, no lineshape could be observed and the γ-ray peaks contain only fully-stopped components).

Level lifetimes were extracted using a code based on that of Wells and Johnson [19]. The analysis was carried out in three steps:

(i) Monte Carlo simulations of the "slowing histories" of ^{192}Pb recoils in the Er target and Pb backing were performed. Five thousand such histories were produced, spanning a total of 2.16 ps in steps of 1.2 fs. The simulation included multiple scattering, electronic and nuclear stopping effects. The stopping powers were calculated using the tables of Ziegler [20].

(ii) The resulting velocity distributions were combined with the detector geometries to produce theoretical lineshapes for all decay times and all angles.

(iii) The theoretical lineshapes were combined with information about transition energies, side-feeding models, and side-feeding intensities; the resulting lineshapes were fitted to the triple-gated spectra for different rings of detectors in a χ^2-minimization.

The side-feeding was modelled by rotational cascades with a moment of inertia the same as the SD band at rotational frequency $\hbar\omega \approx 0.2$ MeV ($\Im^{(2)} = 100\ \hbar^2$/MeV). This model was chosen on the assumption that the yrast SD band will be predominantly fed from excited states within the SD well. It was found that variations in the choice of this moment of inertia of up to 20% had a negligible effect on the results. The results were more sensitive to the number of transitions in the cascade—the cascade length giving the minimum χ^2 and adopted in the final analysis was two, which is smaller than the length adopted in DSAM analyses of other SD bands in Hg and Pb isotopes. The shorter side-feeding cascades may be explained by the higher fissility of this neutron-deficient nucleus compared to the heavier neighbours and the lower-Z mercury isotopes. This results in a reduced cross-section at high spins. The spectra shown in Figs. 1 and 2 indicate that the population of states in the SD band drops very rapidly with increasing spin, as the competition from fission increases.

Due to the overlap of some of the SD transitions with transitions in the normal part of the decay scheme, it was also necessary to include ND stopped peaks in the fitting procedure for all SD transitions except the 535 keV and 345 keV γ rays. Transitions at 502 and 504 keV, originating from low-spin transitions in the normal decay of ^{192}Pb, were included in the fit to the 499 keV $24^+ \rightarrow 22^+$ SD transition. Similar transitions at 463 keV and 383 keV were included in the fit to the 462 keV and 385 keV SD transitions, respectively. A 416 keV transition associated with ^{190}Hg and brought into the spectra by the 262, 304, 385 and 535 keV gates was included in the fit to the 424 keV SD transition. The centroids of these peaks were measured in spectra which were not gated on the SD band. These values

were used as input into the subsequent lineshape fits, and the intensities of the stopped contaminants were free parameters.

Once the information regarding side-feeding and contaminant peaks was established, the fit to the data was carried out with the in-band and side-feeding quadrupole moment as free parameters. In all cases, the theoretical curves were fitted to data from detectors at five angles ($\theta = 31.7°$, $37.4°$, $142.6°$, $148.3°$ and $162.7°$) simultaneously.

Initially, the lifetime of each level was fitted individually. The lifetime of the 535 keV ($26^+ \rightarrow 24^+$) SD transition was fitted first, and the results of this fit were used as input in fitting the lifetime of the subsequent 499 keV ($24^+ \rightarrow 22^+$) SD transition. This procedure was repeated iteratively for all transitions down to the 345 keV ($16^+ \rightarrow 14^+$) γ ray. In this process, it was found that the best fits were obtained when the side-feeding quadrupole moment Q_{sf} was equal to or about 10% less than the in-band quadrupole moment Q_t. It was also found that the lifetime of the lowest level included in the fit could not be measured.

Following this, the lifetimes of all levels were fitted simultaneously, starting with the 26^+ level and adding the lower-lying levels until all states were included. When the side-feeding and in-band quadrupole moments were both treated as free parameters, the values differed significantly for the 462 and 424 keV transitions. However, the fits to these peaks in the simultaneous fit procedure is complicated by the need to fit fully-stopped ND lines which overlap with the partially-shifted SD lines. The 462 keV transition is fed by the 499 keV transition, which must be fitted using a multi-peak fit due to its overlap with the strong ND 502 and 504 keV transitions. Similarly, the 462 keV SD transition itself overlaps with an intense, fully-stopped ND peak. This resulted in large uncertainties and broad minima in the χ^2 surface. Thus as a final step, all transitions were fitted simultaneously but with constant, fixed Q_{sf}. The fit was repeated for values of Q_{sf} between 15 and 24 eb in steps of 0.1 eb. The best fit was obtained with $Q_{sf} = 19.0$ eb, but the χ^2 was found to be very flat for values between 17.8 and 20.1 eb. The SD Q_t values were then determined by a simultaneous fit to all levels in the SD band in the region $26\hbar \geqslant I \geqslant 18\hbar$. Examples of the lineshapes obtained in this way are shown in Figs. 3 and 4.

5. Results

The Q_t values obtained in this analysis are given in Table 1. This final fit, in which all parameters were fixed to previously-fitted values except for the transition lifetimes, resulted in $\chi^2_{\nu=749} = 1.04$.

Measurements of the lifetimes of the lowest levels in other SD bands in this mass region [21] indicate that the deformation is constant to the lowest observed spins. Assuming a constant deformation here, the values of Q_t given in Table 1 are consistent with $Q_t = 19.6^{+0.5}_{-0.4}$ eb, where the errors reflect the statistical uncertainty in the weighted average. The uncertainty in the stopping powers contribute an additional 10% systematic error. Despite this uncertainty, it is interesting to compare the present result with the quadrupole moments measured for the heavier isotopes [15], particularly since the stopping material in that work was also Pb, and the same stopping powers [20] were also used.
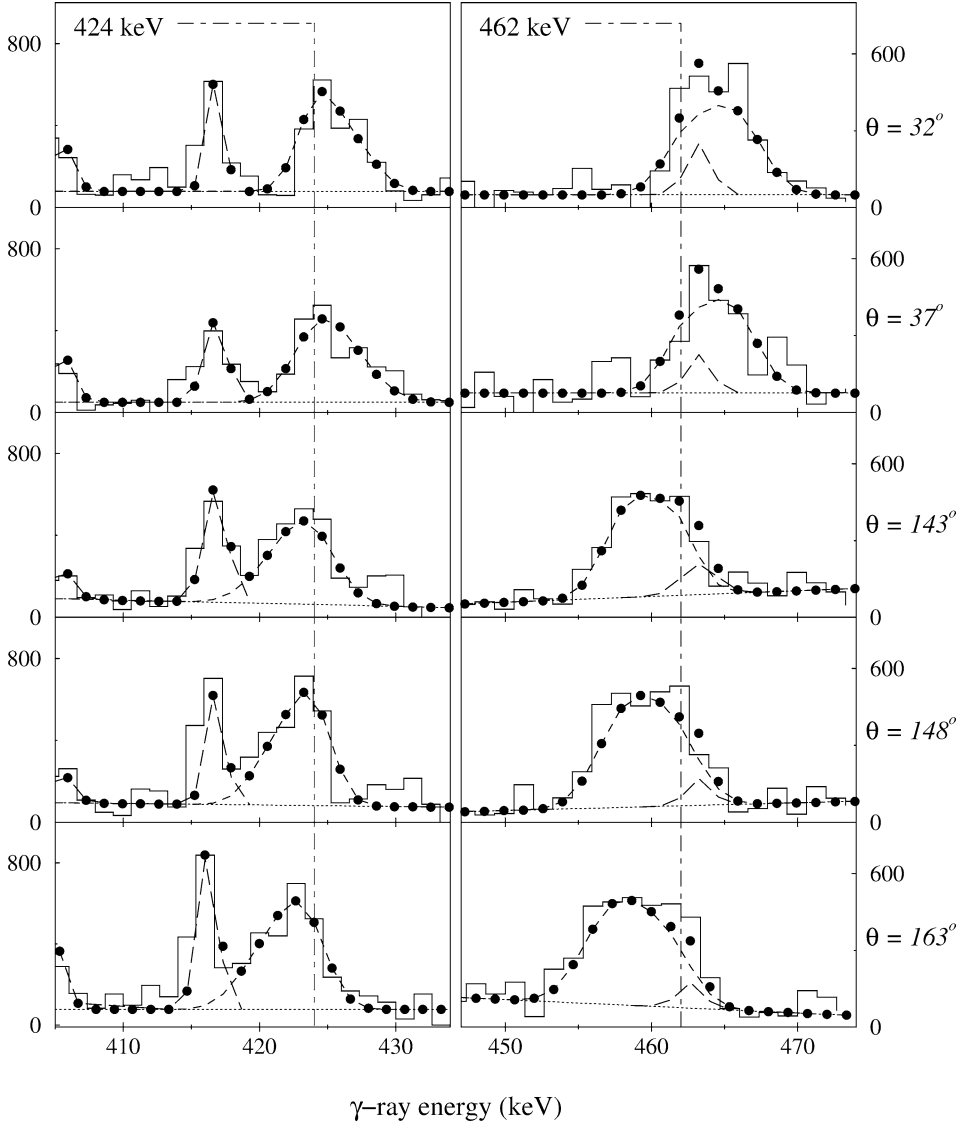
Fig. 3. Fits of theoretical lineshapes to the 424 and 462 keV transitions. Fits to contaminant/stopped transitions are indicated by long-dashed lines; fits to the shifted SD transitions are shown by short-dashed lines; total fits are indicated by filled circles.

6. Discussion

6.1. Previous interpretation of the SD Pb quadrupole moments

In their comparative measurement of the lifetimes of the yrast SD bands in ^{193}Pb to ^{196}Pb, van Severen et al. [15] found remarkably consistent quadrupole moments of $Q_t \approx$
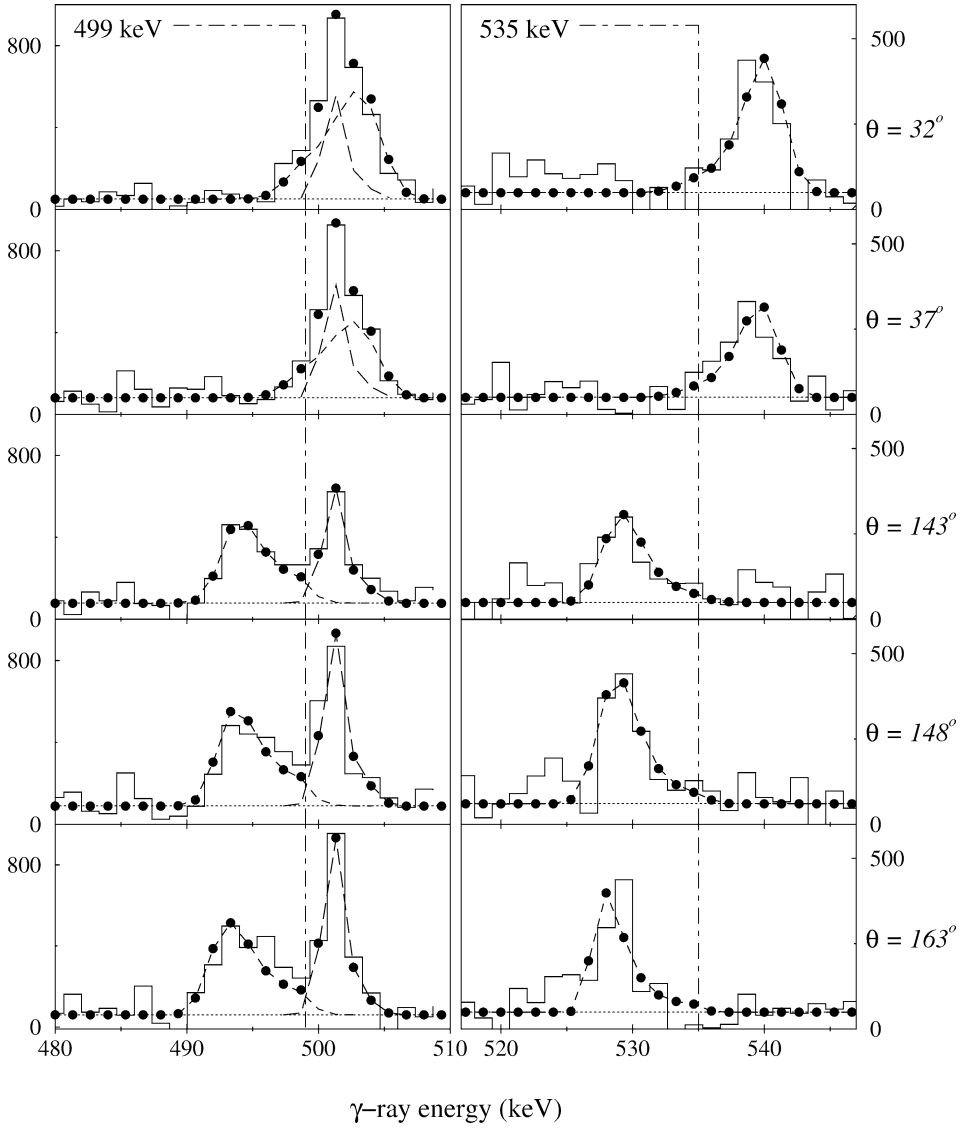
Fig. 4. Fits of theoretical lineshapes to the 499 and 535 keV transitions. (See caption to Fig. 3).

Table 1
Values of Q_t obtained for levels in the yrast SD band in ^{192}Pb

	Spin of initial level ($\hbar$)				
	26	24	22	20	18
Q_t (eb)	$19.0^{+0.68}_{-0.67}$	$19.2^{+1.14}_{-0.7}$	$21.61^{+1.48}_{-1.3}$	$20.86^{+1.56}_{-1.49}$	$21.64^{+3.05}_{-2.61}$

19.5–20.1 eb for all isotopes with mass $N \geqslant 112$. The value obtained for ^{193}Pb, however, was measured to be significantly less than the heavier neighbours, with $Q_t = 17.3(7)$ eb. This difference (around 15%) is much larger than the 4% statistical uncertainty in the measurements of the individual moments. The reduction in the deformation was attributed to a smaller number of intruder orbitals occupied in the lighter nucleus. In that work, intruder-orbital configuration assignments were suggested such that in ^{193}Pb, only one signature of the 7_2 pair (described as of [761]3/2 origin) is occupied, whereas both signatures are occupied in all the heavier isotopes.

6.2. Total Routhian surface calculations and the second minimum in the Pb isotopes

In a naive single-particle interpretation, one would therefore expect the lowest-energy yrast state in ^{192}Pb to involve occupation of neither signature of the 7_2 orbital. If this were the case, and the intruder-orbital occupation was the determining factor, it would be expected that this lightest isotope would also have a reduced quadrupole moment, perhaps even smaller than that of ^{193}Pb. However, it is well-established that pairing is important in the SD bands in this mass region [22] and thus explanations which do not take pairing into account are not appropriate. In order to fully understand the reduction in Q_t observed in ^{193}Pb, and to establish whether a reduced Q_t should be expected in ^{192}Pb, we have investigated the potential energy surfaces and quasi-particle configurations in the Pb isotopes with $110 \leqslant N \leqslant 114$. Total Routhian surface (TRS) calculations employing a Woods–Saxon potential were performed for the vacuum configurations of ^{192}Pb, ^{194}Pb and ^{196}Pb, and for the negative parity single-quasineutron configurations in ^{193}Pb and ^{195}Pb. The TRS method is described in detail elsewhere [23]; in essence, the total Routhian of the nucleus for a given quasiparticle configuration is minimized with respect to the deformation parameters β_2, β_4, and γ, at steps in rotational frequency ω, resulting in a TRS for each frequency. Each TRS has a well-defined parity and signature, but no other quantum numbers are conserved. Examples of the resulting surfaces calculated at rotational frequencies corresponding to spins of $\approx 25\hbar$ in the SD minimum are shown in Fig. 5.

The second minimum responsible for the SD states is clearly visible in each case close to $\beta_2 = 0.475$. In ^{196}Pb, a minimum is evident at $\beta_2 \approx 0.475$ at $\hbar\omega = 0.0$ which becomes yrast at spins in the SD well around $I = 50\hbar$. In ^{195}Pb, this minimum moves to lower deformation at the highest spins, with β_2 decreasing to 0.44 by $I = 70\hbar$, but the deformation remains stable over the spins in which the SD bands are observed experimentally. In ^{194}Pb, the second minimum is calculated to occur at the marginally larger deformation of $\beta_2 = 0.485$, and as in the $N = 114$ case, the deformation remains remarkably stable over all rotational frequencies. In ^{192}Pb and ^{193}Pb, although the SD minimum (at $\beta_2 \approx 0.475$) is visible at $\hbar\omega = 0.0$, it is significantly shallower than in the heavier isotopes. In ^{193}Pb, this minimum stays at the same deformation to the highest calculated rotational frequencies, whereas for ^{192}Pb the calculations suggest that the deformation is reduced to $\beta_2 \approx 0.43$ by $I \approx 50\hbar$, where the minimum becomes yrast. However, as the SD band in this nucleus is not populated above $I \approx 40\hbar$ in the reaction used in this work, the observed SD band can be assumed to correspond to the region where the deformation is stable and $\beta_2 \approx 0.47$ (3% less than in ^{194}Pb). The positions of the superdeformed minima obtained in these calcu-
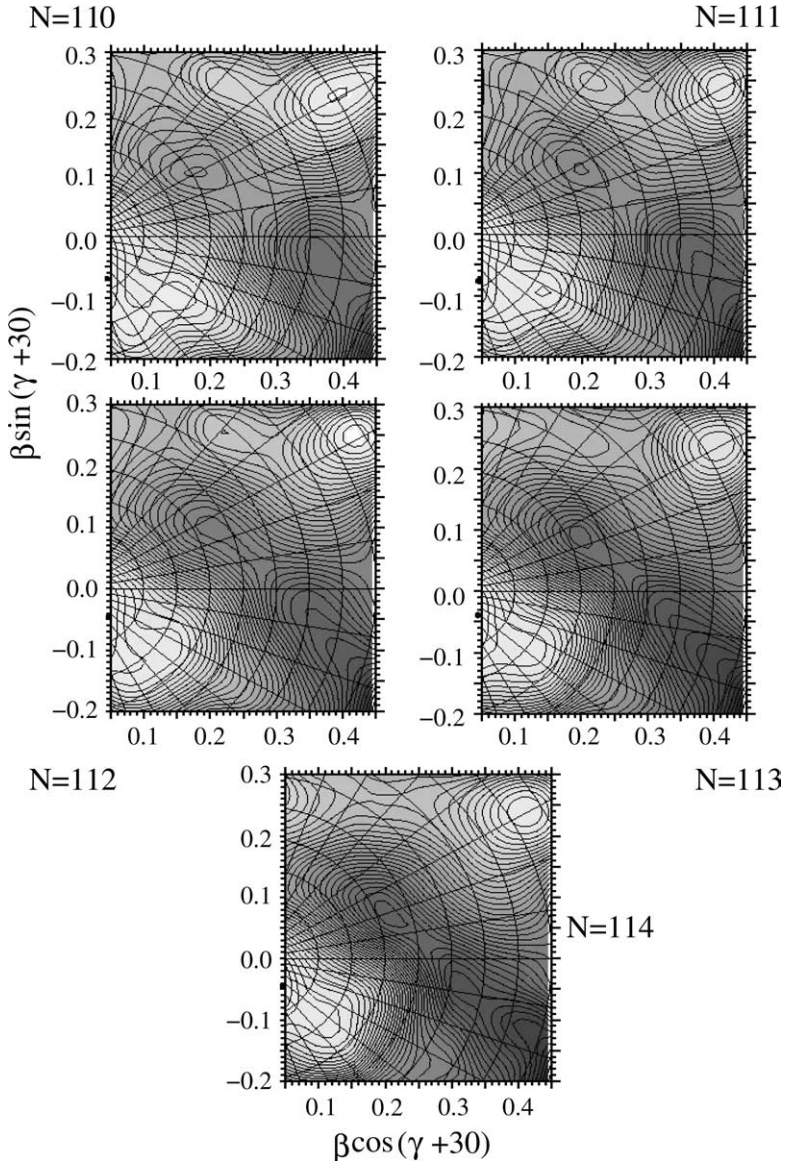
Fig. 5. Examples of the results of the TRS calculations performed for the Pb isotopes with $110 \leqslant N \leqslant 114$. Surfaces are shown for each isotope for spins close to $I = 25\hbar$. The contours spacing is 200 keV.

lations thus suggest no significant change in the deformation of the yrast SD states as the neutron number decreases.

Calculations of the quasiparticle orbitals close to the Fermi surface of these nuclei at $\beta_2 = 0.47$ have also been performed, using the methods described in Refs. [24,25]. These show that the orbitals which are closest to the Fermi surface are the 7_2 state (which is

predominantly of $3/2^-[761]$ character, but has a large admixture of $5/2^-[752]$); the 7_3 state (a highly mixed state with large admixtures of $1/2^-[770]$ and $3/2^-[761]$ states); and the $5/2^-[512]$ and $7/2^-[514]$ orbitals of $f_{7/2}$ and $h_{9/2}$ origin.

Arguments based on experimental moments of inertia, Routhians and signature splitting have been used to identify the yrast SD band in ^{193}Pb with the single quasineutron $3/2^-[761]$ excitation [15,16], meaning that the single neutron occupies the favoured signature of the 7_2 pair. This assignment is the foundation of the interpretation of the lower deformation as being due to the occupation of fewer intruder orbitals. However, this contradicts the results of the TRS calculations above, and in any case may be an unrealistic expectation. One might expect that the minimum become shallower (and consequently softer) with decreasing neutron number, as the Fermi surface moves further from the intruder orbitals and the probability of scattering into them by the pairing interaction becomes smaller. This is indeed what is observed in the TRS calculations. When the SD states have spin $I \approx 25\hbar$, the minimum at $\beta_2 \approx 0.47$ has a depth of around 1.8 MeV in ^{194}Pb; this reduces to 1.5 MeV ^{193}Pb and still further to 1.1 MeV in ^{192}Pb. In ^{193}Pb, the occupation of only one signature of the 7_2 pair blocks scattering into that pair, and thus the well-depth is decreased. In ^{192}Pb, the increasing distance from the Fermi surface of both the 7_2 and 7_3 orbitals results in a decreased probability of scattering into those orbitals by the pairing interaction, thus lowering their occupation probability and again reducing the depth of the SD well. However, as noted above, the minimum remains centred at almost the same β_2 in each case. That is, a shallower well should not result in a lower deformation in the absence of any other influences on the nuclear shape.

6.3. A third minimum in the Pb isotopes with $N \leqslant 112$

It is therefore necessary to investigate other possible causes for the significant reduction in the quadrupole moment observed for ^{193}Pb compared to the heavier neighbours, and try to determine whether a "normal" or "reduced" superdeformation should be observed in SD ^{192}Pb. Closer inspection of the potential energy surfaces shown in Fig. 5 shows that in the isotopes with $N \leqslant 112$ a third minimum develops at $\beta_2 \approx 0.33$, $\gamma \approx 20°$. This minimum first appears as a shallow "spur" off the SD minimum around $\hbar\omega = 0.32$ in the even-N nuclei and $\hbar\omega = 0.24$ in the odd-N nucleus, corresponding to SD states with $I = 20\hbar$. In all three cases, it gradually deepens and becomes better defined with increasing rotational frequency. In the region over which the DSAM measurements of the quadrupole moments are made, the minimum is somewhat better developed in ^{193}Pb. This minimum does not appear in the calculations for the heavier isotopes at any frequency.

The orbitals close to the Fermi surface at $\beta_2 = 0.33$, $\gamma = 20°$ are the same $5/2^-[512]$ and $7/2^-[514]$ orbitals which are close to the Fermi surface for the SD shape. It is thus possible that mixing between states with a strong $N = 5$ component in this minimum and the SD minimum could affect the deformation of the SD bands. This effect might be expected to be least profound in ^{194}Pb, where the SD minimum is deepest and the third minimum very shallow. The relative depths of the two minima in ^{192}Pb and ^{193}Pb are similar, and thus a reduced deformation might be expected in both of these lighter nuclei, but the third minimum is most pronounced in ^{193}Pb and so the effect in each of these two nuclei will be somewhat different. It should again be noted that the TRS calculations are performed for

fixed rotational frequency—in order to make a more quantitative assessment of the effect of the third minimum, calculations performed for fixed spin are required. Detailed calculations of this nature, which are beyond the scope of the current work, would be required in order to predict precise deformations in each of these three cases. However, the presence of this third minimum does suggest a possible factor which, combined with the decreasing stability of the SD minimum, might cause a significant reduction in the deformation of the SD nucleus.

In summary, the transition quadrupole moment of the yrast SD band in ^{192}Pb has been measured using the DSAM lineshape technique. The result is consistent with a constant quadrupole moment of $Q_t = 19.6^{+0.5}_{-0.4}$, where the errors refer only to the statistical uncertainty. Because of the additional systematic uncertainty, it is not possible to determine whether this value is similar to those of the heavier Pb isotopes with $N \geqslant 112$, or whether it is more like that of the $N = 111$ neighbour. Woods–Saxon calculations have been performed with the aim of understanding the deformations of the superdeformed Pb isotopes. These calculations do not indicate a lessening of the β_2 associated with the SD minimum with decreasing N in the Pb isotopes. However, they reveal the presence of a third minimum, at $\beta_2 = 0.33$, $\gamma = 20°$, in the isotopes with $N = 110, 111$ and 112. It is suggested that this minimum, combined with the relative softness of the SD minimum, may contribute to the reduction of the deformation in ^{193}Pb compared to the heavier neighbours. In order to understand the interaction of the different minima, more detailed calculations, in which the potentials are calculated at fixed spin, are needed. It is not clear whether a similar reduction should also be expected in ^{192}Pb. The current data are not sufficient to determine whether the quadrupole moment of SD ^{192}Pb is the same as, or less than, that of isotopes with $N \geqslant 112$. A simultaneous measurement of the moments of SD ^{192}Pb, ^{193}Pb and ^{194}Pb is required if this is to be accurately determined.

Acknowledgements

References

[1] E.F. Moore, R.V.F. Janssens, R.R. Chasman, I. Ahmad, T.L. Khoo, F.L.H. Wolfs, D. Ye, K.B. Beard, U. Garg, M.W. Drigert, Ph. Benet, Z.W. Grabowski, J.A. Cizewski, Phys. Rev. Lett. 63 (1989) 360.
[2] B. Singh, R. Zywina, R.B. Firestone, Nucl. Data Sheets 97 (2002) 241.
[3] T.L. Khoo, M.P. Carpenter, T. Lauritsen, D. Ackermann, I. Ahmad, D.J. Blumenthal, S.M. Fischer, R.V.F. Janssens, D. Nisius, E.F. Moore, A. Lopez-Martens, T. Døssing, R. Krücken, S.J. Asztalos, J.A. Becker, L. Bernstein, R.M. Clark, M.A. Deleplanque, R.M. Diamond, P. Fallon, L.P. Farris, F. Hannachi, E.A. Henry, A. Korichi, I.Y. Lee, A.O. Macchiavelli, F.S. Stephens, Phys. Rev. Lett. 76 (1996) 1583.

[4] G. Hackman, T.L. Khoo, M.P. Carpenter, T. Lauritsen, A. Lopez-Martens, I.J. Calderin, R.V.F. Janssens, D. Ackermann, I. Ahmad, S. Agarwala, D.J. Blumenthal, S.M. Fischer, D. Nisius, P. Reiter, J. Young, H. Amro, E.F. Moore, F. Hannachi, A. Korichi, I.Y. Lee, A.O. Macchiavelli, T. Døssing, T. Nakatsukasa, Phys. Rev. Lett. 79 (1997) 4100.

[5] A. Lopez-Martens, F. Hannachi, A. Korichi, C. Schuck, E. Gueorguieva, Ch. Vieu, B. Haas, R. Lucas, A. Astier, G. Baldsiefen, M. Carpenter, G. de France, R. Duffait, L. Ducroux, Y. Le Coz, Ch. Finck, A. Görgen, H. Hübel, T.L. Khoo, T. Lauritsen, M. Meyer, D. Prevost, N. Redon, C. Rigollet, H. Savajols, J.F. Sharpey-Schafer, O. Stezowski, Ch. Theisen, U. van Severen, J.P. Vivien, A.N. Wilson, Phys. Lett. B 380 (1996) 18.

[6] K. Hauschild, L.A. Bernstein, J.A. Becker, D.E. Archer, R.W. Bauer, D.P. McNabb, J.A. Cizewski, K.-Y. Ding, W. Younes, R. Krücken, R.M. Diamond, R.M. Clark, P. Fallon, I.-Y. Lee, A.O. Macchiavelli, R. MacLeod, G.J. Schmid, M.A. Deleplanque, F.S. Stephens, W.H. Kelly, Phys. Rev. C 55 (1997) 2819.

[7] A.N. Wilson, G.D. Dracoulis, A.P. Byrne, P.M. Davidson, G.J. Lane, R.M. Clark, P. Fallon, A. Görgen, A.O. Macchiavelli, D. Ward, Phys. Rev. Lett. 90 (2003) 142501.

[8] M.J. Joyce, J.F. Sharpey-Schafer, P.J. Twin, C.W. Beausang, D.M. Cullen, M.A. Riley, R.M. Clark, P.J. Dagnall, I. Deloncle, J. Duprat, P. Fallon, P.D. Forsyth, N. Fotiades, S.J. Gale, B. Gall, F. Hannachi, S. Harissopulos, K. Hauschild, P.M. Jones, C.A. Kalfas, A. Korichi, Y. Le Coz, M. Meyer, E.S. Paul, M.G. Porquet, N. Redon, C. Schuck, J. Simpson, R. Vlastou, R. Wadsworth, Phys. Rev. Lett. 71 (1993) 2176.

[9] J. Duprat, F. Azaiez, C. Bourgeois, J.F. Sharpey-Schafer, M.G. Porquet, M. Aiche, C.W. Beausang, R.M. Clark, I. Deloncle, R. Duffait, B. Gall, S.J. Gale, F. Hannachi, I. Hibbert, M.J. Joyce, M. Kaci, W.H. Kelly, A. Korichi, Y. Le Coz, M. Meyer, N. Perrin, N. Poffe, N. Redon, H. Sergolle, C. Schuck, J. Simpson, R. Wadsworth, Phys. Lett. B 341 (1994) 6.

[10] S. Bouneau, A.N. Wilson, F. Azaiez, J.F. Sharpey-Schafer, A. Korichi, I. Deloncle, M.-G. Porquet, J. Timár, A. Astier, M. Bergström, C. Bourgeois, L. Ducroux, J. Duprat, B.J.P. Gall, F. Hannachi, M. Kaci, Y. Le Coz, A. Lopez-Martens, M. Meyer, E.S. Paul, N. Perrin, S. Pilotte, N. Redon, M.A. Riley, C. Schuck, H. Sergolle, R. Wyss, Phys. Rev. C 53 (1996) R9.

[11] D. Rossbach, A.N. Wilson, C. Barton, M.P. Carpenter, D.M. Cullen, H. Hübel, R.V.F. Janssens, S.L. King, A. Korichi, A.T. Reed, Nucl. Phys. A 660 (1999) 393.

[12] J.F. Ziegler, Appl. Phys. Lett. 31 (1977) 544.

[13] E.F. Moore, T. Lauritsen, R.V.F. Janssens, T.L. Khoo, D. Ackermann, I. Ahmad, H. Amro, D. Blumenthal, M.P. Carpenter, S.M. Fischer, G. Hackman, D. Nisius, F. Hannachi, A. Lopez-Martens, A. Korichi, S. Asztalos, R.M. Clark, M.A. Deleplanque, R.M. Diamond, P. Fallon, I.Y. Lee, A.O. Macchiavelli, F.S. Stephens, J.A. Becker, L. Bernstein, L.P. Farris, E.A. Henry, Phys. Rev. C 55 (1997) R2150.

[14] B.C. Busse, P. Fallon, R. Krücken, D. Ackermann, I. Ahmad, S.J. Asztalos, D.J. Blumenthal, M.P. Carpenter, R.M. Clark, M.A. Deleplanque, R.M. Diamond, S.M. Fischer, F. Hannachi, R.V.F. Janssens, T.L. Khoo, A. Korichi, T. Lauritsen, I.Y. Lee, A. Lopez-Martens, A.O. Macchiavelli, R.W. MacLeod, E.F. Moore, D. Nisius, G. Schmid, D. Seweryniak, F.S. Stephens, K. Vetter, Phys. Rev. C 57 (1998) R1017.

[15] U.J. van Severen, R.M. Clark, R. Krücken, H. Hübel, S.J. Asztalos, J.A. Becker, B.C. Busse, M.A. Deleplanque, R.M. Diamond, P. Fallon, K. Hauschild, I.M. Hibbert, I.Y. Lee, A.O. Macchiavelli, R.W. MacLeod, G. Schmid, F.S. Stephens, K. Vetter, R. Wadsworth, S. Wan, Phys. Lett. B 434 (1998) 14.

[16] D. Rossbach, A. Görgen, H. Hübel, E. Mergel, G. Schönwasser, F. Azaiez, C. Bourgeois, F. Hannachi, A. Korichi, A. Lopez-Martens, A. Astier, N. Buforn, N. Redon, O. Stezowski, D. Bazzacco, T. Kroll, C. Rossi-Alvarez, K. Hauschild, W. Korten, R. Lucas, H.J. Maier, P. Reiter, P.G. Thirolf, Phys. Rev. C 66 (2002) 024316.

[17] P. Fallon, F.S. Stephens, S. Asztalos, B. Busse, R.M. Clark, M.A. Deleplanque, R.M. Diamond, R. Krücken, I.Y. Lee, A.O. Macchiavelli, R.W. MacLeod, G. Schmid, K. Vetter, T. Nakatsukasa, Phys. Rev. C 55 (1997) R999.

[18] I.Y. Lee, Nucl. Phys. A 520 (1990) 641c.

[19] J.C. Wells, N. Johnson, Lineshape: a computer program for Doppler-broadened line-shape lifetime analysis, Oak Ridge National Lab. Report No. ORNL-6689 (1991) 44.

[20] J.E. Ziegler, J.P. Biersack, U. Littmark, The Stopping and Ranges of Ions in Matter, Pergamon, London, 1985.

[21] R. Krücken, S.J. Asztalos, J.A. Becker, B. Busse, R.M. Clark, M.A. Deleplanque, A. Dewald, R.M. Diamond, P. Fallon, K. Hauschild, I.Y. Lee, A.O. Macchiavelli, R.W. MacLeod, R. Peusquens, G.J. Schmid, F.S. Stephens, K. Vetter, P. von Brentano, Phys. Rev. C 55 (1997) R1625, and references therein.
[22] R.V.F. Janssens, T.L. Khoo, Annu. Rev. Nucl. Part. Sci. 41 (1991) 321.
[23] R. Wyss, J. Nyberg, A. Johnson, R. Bengtsson, W. Nazaerwicz, Phys Lett. B 215 (1989) 211;
W. Nazarewicz, G.A. Leander, A. Johnson, Nucl. Phys. A 503 (1989) 285.
[24] W. Nazarewicz, J. Dudek, R. Bengtsson, I. Ragnarsson, Nucl. Phys. A 435 (1985) 397.
[25] S. Cwiók, J. Dudek, W. Nazarewicz, W. Skalski, T. Werner, Comput. Phys. Commun. 46 (1987) 379.